An optical study on C_{60} vapour, microcrystal beam and film

1998 J. Phys.: Condens. Matter 10 2347

(http://iopscience.iop.org/0953-8984/10/10/015)

J. Phys.: Condens. Matter **10** (1998) 2347–2361. Printed in the UK PII: S0953-8984(98)87289-5

An optical study on C_{60} vapour, microcrystal beam and film

Shosuke Mochizuki†, Mie Sasaki and Raphael Ruppin‡

Department of Physics, College of Humanities and Sciences, Nihon University, 3-25-40 Sakurajosui, Setagaya-ku, Tokyo 156, Japan

Received 1 September 1997

Abstract. During evaporation of C_{60} powder in confined noble gas, flowing noble gas and vacuum, the optical absorption spectra of vapour zones, microcrystal beam and film on a substrate were measured as functions of the time elapsed since the beginning of the evaporation. The results show clearly the spectral evolution from C_{60} molecule to solid. Also, to clarify the details of the optical excitation and relaxation in the condensed C_{60} solid, the absorption, photoluminescence and photoconduction spectra were measured for C_{60} films at various temperatures from 7 K to room temperature.

1. Introduction

The optical properties of C_{60} have attracted much attention recently, because of the fact that doping the crystals with alkali-metal atoms and halogen atoms produces high-temperature superconductors and ferromagnets, respectively. Understanding these interesting properties requires detailed information on the electronic structure of pristine C_{60} crystal. At present, however, the electronic structure is still debated. For example, even the band-gap energy E_g is assigned a wide range of values (1.6 eV $< E_g <$ 2.3 eV) by various workers (Mishori *et al* 1997, Milani *et al* 1994, Capozzi *et al* 1996, Lof *et al* 1992), who have employed mainly optical and photoelectron spectroscopies. Theoretically, Ohno *et al* (1996) showed that the gap energy and the widths of the bands are quite sensitive to the molecular orientation in the crystal. In order to resolve these issues, it is useful to study how the structure of the optical spectrum of the aggregates $(C_{60})_n$ changes with increasing number n of the constituent molecules.

We gradually elevated the temperature of C_{60} powder in confined noble gas, in flowing noble gas and in vacuum with a high velocity to produce vapour, microcrystals and films, respectively. Since the concentration of the vapour species of C_{60} increases with increasing temperature, the film thickness and crystallite size increase over time. During the evaporation, the optical absorption spectra of vapour zones, microcrystal beam and film on a substrate were measured *in situ* as functions of the time elapsed since the beginning of the evaporation. The results show a clear spectral evolution from C_{60} molecule to solid.

† Author to whom any correspondence should be addressed; telephone: 03-5317-9733; fax: 03-5317-9432; e-mail: motizuki@phys.chs.nihon-u.ac.jp.

‡ Present address: Department of Physics and Applied Mathematics, Soreq NRC, Yavne 81800, Israel.

0953-8984/98/102347+15$19.50

2. Experimental procedure

The starting material is nominally pure powder (purity 99.98%, TERM USA; main impurity: C_{70}). Before the evaporation was carried out, the powder was degassed under vacuum for several hours to remove residual solvent and adsorbed impurities.

The production and absorption measurements on the C_{60} vapour zones and microcrystal beam were carried out with an apparatus used for free-metal and semiconductor microcrystal studies (Mochizuki and Ruppin 1993, Mochizuki 1996, Mochizuki and Umezawa 1997) as follows.

The C_{60} vapour zone was produced by heating the powder gradually in helium or argon gas confined at a pressure between 50 and 300 Torr. For producing C_{60} microcrystal beam, a gas stream with a high velocity was made by introducing argon gas continuously into the bottom of the evaporation chamber and evacuating a beam chamber with a mechanical booster pump (with an exhaust speed of 1000 l min^{-1}). The temperature of the crucible containing the nominally pure C_{60} powder was gradually increased by applying a constant voltage. The transmissivity spectra of selected positions in the vapour and beam zone were recorded as functions of the time elapsed since the beginning of the evaporation. Continuum light from a 150 W Xe lamp was directed at the whole vapour zone or beam zone through an optical window without using any lens. After passing the vapour zone or beam zone, only the light passing through a selected position was collected, by a lens, and then introduced into an optical multichannel analyser (O.M.A.). Experiments on quasi-free microcrystals were carried out by introducing a silica substrate into the beam chamber described above. After commencing the evaporation, transmissivity spectra of the substrate were measured as a function of time using the same optical analyser system as was used for the microcrystal beam.

Since the transmissivity spectra T_r obtained from the vapour-zone and microcrystal beam measurements contain the effects of both scattering and absorption, the results obtained are expressed as extinction spectra, $-\log T_r$. Unfortunately, at present, we cannot determine *in situ* the crystallite size in the free microcrystal beam. In order to obtain information on the average crystallite size, we inserted an electron microscope grid covered with a carbon-coated triacetylcellulose film and collected microcrystals for about one second, at various stages of the evaporation. The electron microscopic observations on the microcrystals indicate that the time evolution corresponds to an increase in crystallite size. However, it is known from STM studies of size-selected metal clusters deposited on a substrate surface with very low kinetic energy that these clusters tend to aggregate on the surface, which gives structures with sizes that are not representative of the cluster size in the molecular beam. Therefore, the crystallite sizes in the beam may be smaller than those determined from the electron microscopy.

The transition of the absorption spectra during film growth on a silica glass in vacuum was observed by using the same O.M.A. system and procedure as was used in the microcrystal beam measurements. Special care was taken to avoid obstructive deposition on the optical windows of the evaporation chamber. The vacuum evaporations were carried out at a pressure of about 2.6×10^{-6} Torr. The results are expressed as optical density spectra, $-\log T_r$.

For the absorption and photoluminescence measurements on the films, the specimens were put in a helium closed-cycle cryostat, whose temperature could be varied from 7 K to 300 K. Photoluminescence was excited by different argon-ion laser lines ($\lambda = 457.9$ nm, 465.8 nm, 472.2 nm, 476.5 nm, 488.0 nm, 496.5 nm, 501.7 nm, 514.5 nm and 528.7 nm).

The photoconduction spectra of the vacuum-evaporated films were measured as follows.

Opposed-type electrodes with a separation of 1 mm were made by sputtering gold on the surface of C_{60} film. The photoconduction spectra were measured by the synchronous detection method. The radiation from a 150 W Xe lamp passed through a grating monochromator. Monochromatic light modulated in intensity by a variable-frequency (10 Hz–320 Hz) mechanical chopper was incident on the specimen. The photocurrents excited were measured with a lock-in amplifier over a wavelength range from 300 nm to 800 nm. The light intensity at each wavelength was monitored by a calibrated pyroelectric detector (Oriel 7090 with an absorbing black coating). The photoconduction (photocurrent) spectrum is the signal ratio of the photocurrent to the light intensity thus measured.

3. Results

3.1. The C_{60} vapour zone

Figure 1(a) shows the time evolution of the extinction spectra of a C_{60} vapour zone at a height (h) of 3 mm from the crucible edge. Each measurement was made for 1050 ms at intervals of 980 ms and the total number of spectra is 64. Figure 1(b) shows the 18th, 22nd, 24th and 26th spectra from figure 1(a). The time increases in the curves from bottom to top. At the initial stage of evaporation, an absorption tail and a sharp absorption peak appear at a wavelength shorter than 300 nm and at about 330 nm (3.76 eV), respectively, though they are affected by some noise. No other absorption structure was observed. The 330 nm band is accompanied by a shoulder band at about 350 nm, which may be due to close h_u and h_g levels or due to some splittings of the h_g and t_{1u} levels. The spectrum is very similar to those for organic solution shown in a later section and for the gas phase (Kataura *et al* 1993). The tail and the 330 nm absorption band are assigned to the h_u–h_g and h_g–t_{1u} transitions, respectively, in free C_{60} molecules. The absorption intensity peak wavelength 330 nm is close to that (3.65 eV) observed for C_{60} vapour in vacuum (Kataura *et al* 1993). This shows that the majority vapour species is C_{60} molecules at the early stage of gas evaporation of C_{60} powder. The h_g–t_{1u} peak is blue-shifted by 148 meV from the film value reported by Capozzi *et al* (1996).

As the evaporation progresses, the absorptions described above become prominent, and broad absorption bands appear at wavelengths longer than 400 nm. This absorption band is observed only for film and single crystal, being absent for the molecule. Therefore, the broad band may be due to aggregation of C_{60} molecules. The absorption edge is at about 750 nm (1.65 eV) which is close to that observed in the C_{60} beam and films as shown in later sections. Upon further evaporation, the broad absorption band becomes prominent, which indicates an increase in the number of microcrystals and in crystallite size. Also, it was found that the spectral band width of the h_g–t_{1u} band increased as the evaporation progressed.

On proceeding further with the evaporation, the structure of the vapour zones becomes complicated. After measurement of 34 spectra, we clearly saw thick fluctuating outer zones which enveloped the two vertically separated zones. An extinction intensity jump seen at about 90 000 ms in figure 1(a) indicates the complicated structure in vapour at the later stage of the evaporation.

Also, we measured the extinction spectra of the vapour at different heights from the crucible edge. The typical 18th, 22nd, 24th and 26th spectra measured at a height of 15 mm are shown in the inset. The conditions for the evaporation and optical measurements are the same as those prevailing at a height of 3 mm. The spectral evolution over time is similar to that at a height of 3 mm, but the contributions from the shoulder band of the 330 nm

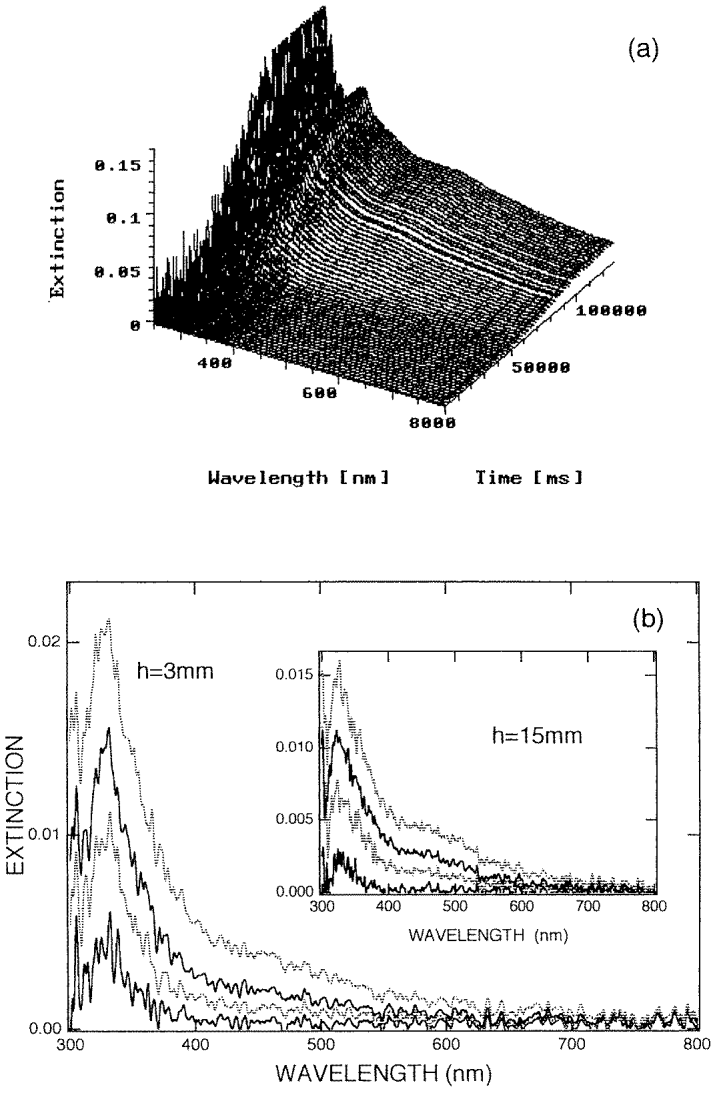

Figure 1. (a) The time evolution of the optical extinction of the C_{60} vapour zone at a height of 3 mm above the crucible edge during gas evaporation under helium gas confined at a pressure of 50 Torr. (b) The 18th, 22nd, 24th and 26th of the time-resolved spectra shown in (a). The inset shows the time evolution of the optical extinction of the C_{60} vapour zone at 15 mm above the crucible edge. The spectra are the 18th, 22nd, 24th and 26th of the time-resolved spectra.

wavelength and the broad band at wavelengths longer than 400 nm are more prominent. During the optical measurements, the temperatures of the vapour zones at the heights 3 mm and 15 mm rose to about 715 K and about 524 K, respectively. These temperatures are lower than that of the experiments made by Kataura *et al* (1993). We performed evaporation under various confined pressures, with various voltages applied to the crucible heater and with different atmosphere gases (helium and argon), but it was more difficult to produce vertically well separated vapour zones of C_{60} than in the case of metals (Mochizuki and Ruppin 1993, 1994, Mochizuki *et al* 1997).

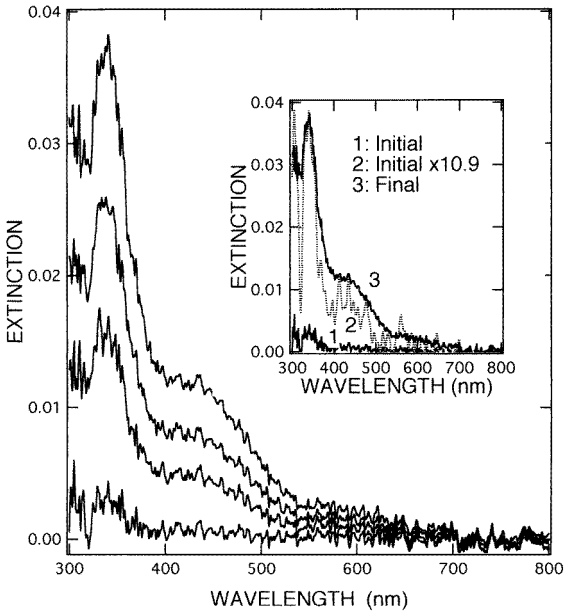

Figure 2. The time evolution of the optical extinction of C_{60} microcrystal beam during evaporation in argon gas with a high velocity. Of 64 spectra, the 20th, 26th, 29th and 36th are shown. The time increases in the curves from bottom to top. The initial (20th) spectrum is compared with the final (36th) one in the inset. They are normalized with respect to the intensity at the peak wavelength of the h_g–t_{1u} band.

3.2. Free C_{60} microcrystals: C_{60} microcrystal beam

Figure 2 shows the 20th, 26th, 29th and 36th of the time-resolved extinction spectra of C_{60} microcrystal beam during the evaporation. The time increases in the curves from bottom to top. Each measurement was made for 1250 ms at intervals of 5000 ms; the total number of spectra is 64. The evaporation was carried out under an argon-gas stream with a flow rate of 10 l min^{-1}. The argon-gas pressure of the evaporation chamber was about 1 Torr. During the optical measurements, the temperature of the beam zone rose to about 314 K. At the initial stage of the evaporation, the absorption tail of the h_u–h_g transition and the absorption band of the h_g–t_{1u} transition appear in the wavelength region below 310 nm and at 340 nm, respectively. The h_g–t_{1u} peak is blue-shifted by 26 meV from the film value reported by Capozzi *et al* (1996). Another weak absorption band appears at about 425 nm. As the evaporation progresses, the absorption intensities of these bands increase. It is noted that the growth rate of the 425 nm band is higher than that of the h_g–t_{1u} band. As the evaporation progresses further, the absorption intensities of these bands increase and weak absorption bands appear at wavelengths longer than 550 nm. To show clearly the evolution of the 425 nm band, the initial (20th) spectrum is compared with the final (36th) one in the inset. They are normalized with respect to the intensity at the peak wavelength of the h_g–t_{1u} band. The 425 nm band may arise from some splitting of degenerate energy levels or electron transfer between neighbouring molecules. A charge-transfer exciton (CT exciton) absorption model was proposed by Tsubo and Nasu (1994). In any case, since it is not observed for the C_{60} molecule, and since it is observed for higher energy than that of the lowest Frenkel exciton, and also since the band width is larger than that (0.5 eV) speculated

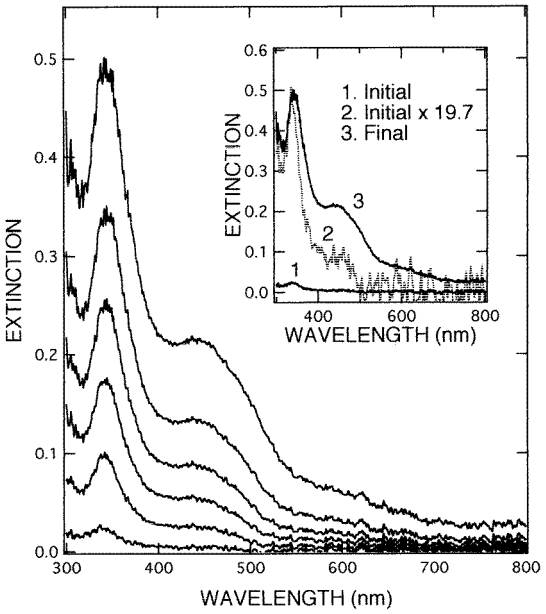

Figure 3. The time evolution of the optical extinction of C_{60} microcrystals on a silica substrate during evaporation in an argon-gas stream with a high velocity. Of 64 spectra, the 34th, 44th, 50th, 54th, 58th and 64th are shown. The time increases in the curves from bottom to top. The initial (34th) spectrum is compared with the final (64th) one in the inset. They are normalized with respect to the intensity at the peak wavelength of the h_g–t_{1u} band.

theoretically for C_{60} solid (Saito and Oshiyama 1991), we call the 425 nm band a CT exciton band. Since the 425 nm band was observed even at the early stages of the evaporation, the CT exciton state may be produced even in small C_{60} microcrystals. Nitta *et al* (1997) have calculated the optical density of C_{60} molecules and C_{60} dimers in which two C_{60} molecules are interacting through long-range electronic interactions. They obtained a solid-like CT exciton absorption spectrum for C_{60} dimers. The weak bands at wavelengths longer than 550 nm are also observed for film and single-crystal specimens. They are characteristic also of the condensed systems of C_{60}.

Electron microscope examinations of microcrystals collected on a carbon-coated triacetylcellulose film at various stages of the evaporation show that their sizes change from several nanometres to several tens of nanometres during the evaporation, though this may be affected by some aggregation between microcrystals on the carbon-coated triacetylcellulose film used for electron microscopy. The shape of the crystallites changes from quasi-spherical to rectangular-like. Also, in order to see the hydrogen-doping effect, we evaporated C_{60} powder in an argon–hydrogen mixture gas stream and measured the extinction spectra, but no new features were observed.

3.3. Quasi-free C_{60} microcrystals: C_{60} microcrystals on a substrate

Figure 3 shows the 34th, 44th, 50th, 54th, 58th and 64th of the time-resolved extinction spectra of C_{60} microcrystals on a silica substrate during the evaporation. The time increases in the curves from bottom to top. The experiment was carried out by introducing the silica substrate into the C_{60} microcrystal beam. The condition of the evaporation was the same

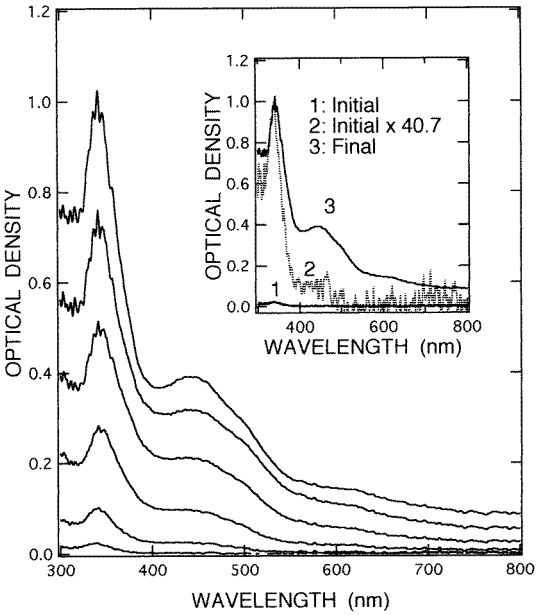

Figure 4. The time evolution of the optical density of C_{60} film on a silica substrate during vacuum evaporation. Of 64 spectra, the 14th, 24th, 34th, 54th and 64th are shown. The time increases in the curves from bottom to top. The initial (14th) spectrum is compared with the final (64th) one in the inset. They are normalized with respect to the intensity at the peak wavelength of the h_g–t_{1u} band.

as that for the microcrystal beam. Each measurement was made for 1050 ms at intervals of 980 ms; the total number of spectra is 64. At the initial stage of the evaporation, the absorption tail of the h_u–h_g transition and the absorption band of the h_g–t_{1u} transition appear at wavelengths shorter than 310 nm and at 340 nm, respectively. The CT exciton absorption band appears at 450 nm, which is red-shifted by 162 meV from the value for the microcrystal beam described above. The CT exciton band shows some structure. With progressing evaporation, the absorption intensities of these bands increase and weak absorption bands appear at wavelengths longer than 550 nm. To show clearly the evolution of the 450 nm and long-wavelength bands, the initial (34th) spectrum is compared with the final (64th) one in the inset. They are normalized with respect to the intensity at the peak wavelength of the h_g–t_{1u} band. Also, as the evaporation progressed, a small red-shift was observed in the h_g–t_{1u} absorption band. The red-shift will be explained later, in section 4.1, on the basis of the increase in crystallite size with progressing evaporation. It is noted that the intensity ratio of the CT absorption band to the h_g–t_{1u} band is higher than that for microcrystal beam. The substrate covered with C_{60} microcrystals was brown/transparent. This may indicate that microcrystals deposited on the substrate at the initial stage of evaporation form an island film and, with increasing coverage ratio of the microcrystals, coalesce to produce a uniform film.

3.4. C_{60} film on a substrate: vacuum evaporation

Figure 4 shows the 14th, 24th, 34th, 44th, 54th and 64th of the time-resolved extinction spectra of C_{60} film on a silica substrate during vacuum evaporation. The time increases in the

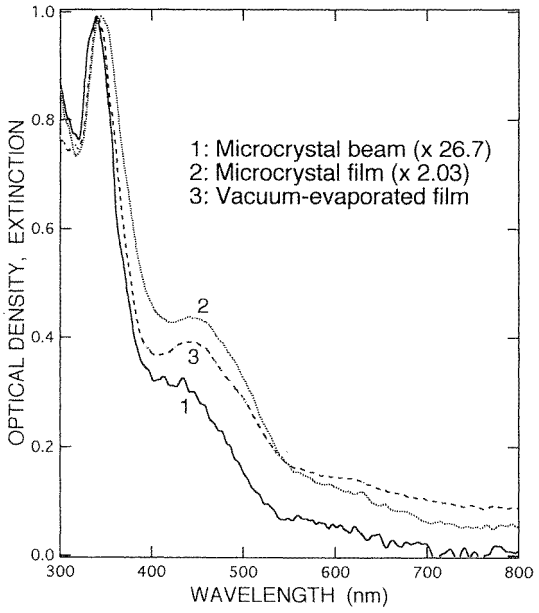

Figure 5. Comparative spectra: C_{60} microcrystal beam, microcrystal film and vacuum-evaporated film at their final stages of evaporation. They are normalized with respect to the intensity at the peak wavelength of the h_g–t_{1u} band.

curves from bottom to top. The final thickness of the film is about 200 nm. The conditions for the optical measurements were the same as those for the microcrystal beam ones. As observed in the experiments on free and supported microcrystals, at the initial stage of the evaporation, the absorption tail of the h_u–h_g transition and the absorption band of the h_g–t_{1u} transition appear at wavelengths shorter than 310 nm and at 340 nm, respectively. Also, the CT exciton absorption band appears at 450 nm, which is red-shifted by 125 meV from the value for the microcrystal beam described above. As the evaporation progressed, a small red-shift was observed in the h_g–t_{1u} absorption band. This red-shift will be explained later, in section 4.1, on the basis of the increase in crystallite size with progressing evaporation. The absorption intensities of these bands increase and weak absorption bands appear at wavelengths longer than 550 nm. A kink at about 625 nm becomes observable. To show clearly the evolution of the 450 nm and long-wavelength bands, the initial (14th) spectrum is compared with the final (64th) one in the inset. They are normalized with respect to the intensity at the peak wavelength of the h_g–t_{1u} band. It is noted that the intensity ratio of the CT absorption band to the h_g–t_{1u} band is higher than that of microcrystal beam, but smaller than that of the supported microcrystals. This band seems to be accompanied by several shoulder bands. Through various vacuum evaporations, it is found that the background absorption at wavelengths longer than 550 nm is specimen dependent, which may be due to the speed of evaporation (Capozzi *et al* 1996) or annealing effects caused by thermal radiation from the evaporation source. The 64th spectrum is very similar to that obtained by Ren *et al* (1991).

Figure 5 shows collectively the spectra of C_{60} microcrystal beam, microcrystal film and vacuum-evaporated film at their final stages of evaporation. They are normalized with respect to the intensity at the peak wavelength of the h_g–t_{1u} band. It is noted that the CT

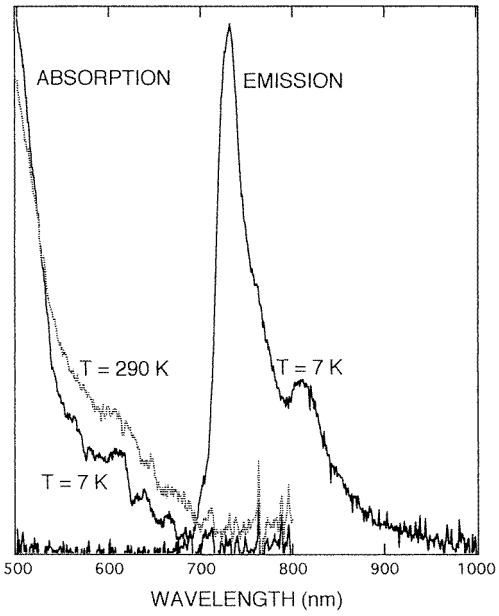

Figure 6. Absorption and photoluminescence spectra of C_{60} film.

exciton absorption band of the C_{60} microcrystal beam is suppressed considerably and is blue-shifted as compared with those for film specimens.

3.5. Optical spectra and photoconduction spectra of C_{60} film

In order to obtain more details on the optical properties of C_{60}, we measured the absorption, photoluminescence and photoconduction spectra of films by the vacuum evaporation method at various temperatures. Figure 6 shows typical absorption (optical density) spectra at 7 K and 290 K and the photoluminescence spectrum at 7 K. The measurements were carried out for the same C_{60} film. The thickness of the film was about 420 nm. The absorption curve intersects the emission one at about 690 nm (1.8 eV). 1.8 eV may be the optical gap of the C_{60} film at 7 K. The photoluminescence spectrum was independent of the excitation light wavelength. In the absorption spectra, the temperature dependence and sideband structures in the wavelength region between 540 nm and 690 nm may originate from some combination excitations of Frenkel excitons and vibrations. The observed separation of about 700 cm^{-1} is close to the frequency of the H_g mode in C_{60} molecules. The photoluminescence spectrum has two distinct peaks at 732 nm and 811 nm, and faint shoulders at 703 nm, 726 nm, 744 nm, 761 nm, 772 nm, 834 nm, 846 nm and 868 nm. The 680 nm emission band due to C_{70} impurities has been reported already by Capozzi *et al* (1996), but we cannot detect such emission.

The photoconduction spectra were measured at various light-intensity modulation frequencies, light intensities and applied voltages. It is found that the photocurrent is proportional to light intensity and applied voltage. Also, it is found that the photocurrent increased with decreasing light-intensity modulation frequency, which may arise from some deep carrier traps in the energy gap. The photocurrent decreases with the time that elapses after applying the voltage, which may be due to some blocking carriers at the electrodes.

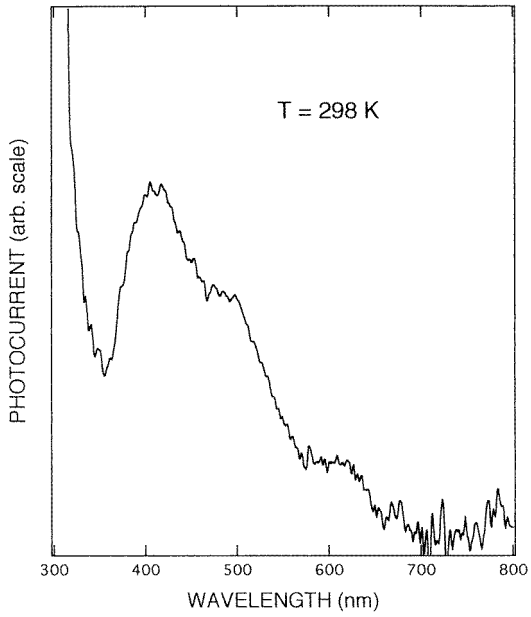

Figure 7. The photoconduction spectrum of C_{60} film at 298 K.

A typical photoconduction spectrum of C_{60} film at 298 K is given in figure 7. The film thickness is the same as that for the absorption and photoluminescence measurements. The spectrum is similar to that of the optical absorption described above, apart from the conduction dip at about 350 nm, and is close to the results obtained by Kazaoui *et al* (1994). A photoconduction edge is observed at about 730 nm (1.7 eV). Although it is not clear at present, such a photoconduction dip appears frequently in intense absorption regions in many photoconductors, which is interpreted as some exciton trapping effect occurring at the specimen surfaces.

4. Discussion

4.1. Electronic states, optical excitation and relaxation of the C_{60} system

When atoms or molecules coalesce to constitute a solid system, the energies of both the ground state and the excited one are lowered, and the excitation energy decreases also. If the solid is a periodic system (a crystal), a molecular excitation can propagate as a Frenkel exciton or a Mott–Wannier one, depending on the extent of the wave function of the excited states. An intermediate type of exciton state is also possible. The excited state is accompanied by charge transfer to neighbouring atoms or molecules, which is called a charge-transfer (CT) exciton. Since, generally, work is needed to transfer charge, CT exciton absorptions are observed on the higher-energy side in the absorption spectra. In molecular solids such as C_{60} condensed systems, the optical spectra are characterized by intra-molecular excitations (Frenkel excitons) and inter-molecular ones (CT excitons). It would be of great interest if one could find answers to the following questions.

(1) How many molecules are needed for such a CT exciton state?

(2) How do the CT exciton and Frenkel exciton states change with increasing number of constituent molecules?

(3) How do such excited (exciton) states relax?

Now, we discuss the absorption, photoluminescence and photoconduction spectra of vacuum-evaporated C_{60} film shown in figures 6 and 7. It is noted that, at wavelengths longer than 600 nm, the absorption and photoluminescence spectra are characterized by some sideband structures. Generally in molecular solids, optical absorption may occur with the assistance of intra-molecular and inter-molecular vibrational energy, i.e., a combined excitation of Frenkel excitons and vibrations. In such a case, some sideband structure appears in the absorption spectrum, the absorption intensity decreases and the structure becomes sharpened with decreasing temperature, as shown in figure 6. The Stokes-shifted broad emission band can be explained by the self-trapped-exciton model. If photogenerated Frenkel excitons stay on C_{60} molecules for a longer time than the periods of the molecular vibrations, they may be trapped by lattice distortion due to strong electron–vibration interaction. In this case, the excitons decay radiatively to excite inter- and intra-molecular vibrations. Therefore, the emission appears at a wavelength longer than that at which absorption occurs, and the spectrum is structured by many phonon peaks and shoulders, as observed. A different interpretation of the structure observed in the photoluminescence spectrum has been given on the basis of noting a resemblance between the photoluminescence spectra of C_{60} film and solution. Friedman and Harigaya (1993) discussed the photoluminescence spectra of a C_{60} molecule using the Su–Schrieffer–Heeger model (Su *et al* 1980). They obtained a series of discrete energy levels separated by 0.21 eV which is close to the energy difference (0.165 eV) between the two distinct emission peaks (732 nm and 811 nm) appearing in figure 6. Also, they predicted several kinds of defect (oxygen impurities, C_{70} impurities and configurational disorder) which make the t_{1u}–h_u transition dipole allowed if the C_{60} film is luminescent. At present, other interpretations cannot be excluded. It is noted that the photoconduction edge was close to about 730 nm (1.7 eV) which was near the intensity peak in the photoluminescence spectra. The similarity between the absorption and photoconduction spectra shows that the Frenkel and CT excitons photogenerated may relax to the same lowest Frenkel exciton state. The Frenkel excitons dissociate to produce carriers by scattering at surfaces or scatterings by vibrations, impurities and defects. Since the Frenkel exciton state is energetically below the conduction state, the conduction has a vibration-assisted nature, i.e., a positive temperature coefficient. Alternatively, since the conduction band width calculated is small (about 0.5 eV), the conduction is thought to be a hopping one via C_{60}^{-} conduction states (Kazaoui *et al* 1994), with a positive temperature coefficient. The fact that the photoconduction edge is lower than the absorption one indicates that there are many levels in the energy gap.

Next, we discuss the spectral evolution of C_{60} microcrystals, $(C_{60})_n$. Prior to the discussion, we show the absorption spectra of a C_{60} film evaporated onto a silica substrate and two kinds of C_{60} solution, in figure 8. The solvents were toluene and various hexanes. The spectral width and intensity peak wavelength of the h_g–t_{1u} band depend on the kind of solvent used, which may be due to some interaction between the C_{60} molecules and the solvent molecules in the environment. The 425 nm band for microcrystal beam and the 450 nm band for film and also the long-wavelength absorption tail structured by some peaks and shoulders are suppressed extremely strongly, and seem to be absent for the solutions and C_{60} vapours (Kataura *et al* 1993). Therefore, it is important to study spectral evolution for wavelengths longer than 400 nm to elucidate the electronic states of C_{60} condensed systems. Aggregation of C_{60} molecules may induce some splitting of degenerate energy levels and electron transfer between neighbouring molecules. Additionally, the parity- and spin-forbidden transitions in the molecular state become partially allowed due to lattice and orientational fluctuations, and vibronic interactions (Yabana and Bertsch 1992) in the C_{60} condensed system. The energy spread due to such a splitting may be within about 0.5 eV,

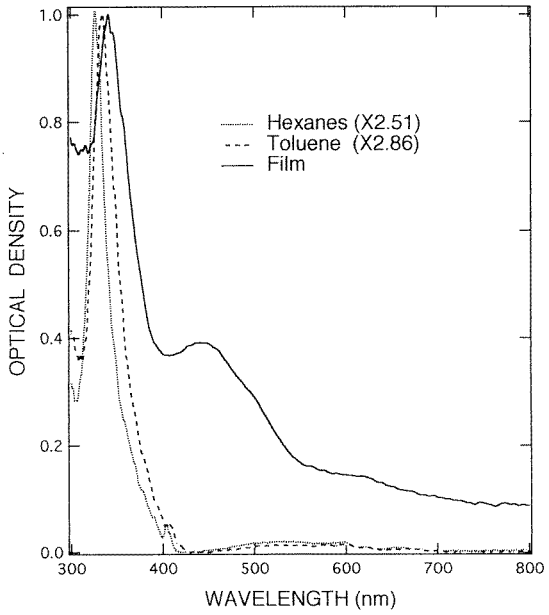

Figure 8. Absorption spectra of C_{60} film evaporated on a silica substrate and two kinds of C_{60} solution.

which is given by the energy band calculation (Saito and Oshiyama 1991, Ohno *et al* 1996). Since the observed widths (about 0.85 eV) of the 425 nm and 450 nm bands are larger than the estimated energy spread, the effects of electron transfer must be considered in the first approximation. The CT exciton is an optical excitation accompanied by an electron transfer. The work required for formation of a CT exciton, W_{CT}, may be given tentatively by

$$W_{CT} = E_I - E_A - e^2/4\pi\varepsilon_0 R \tag{1}$$

where E_I, E_A, e, ε_0 and R are the ionization potential, electron affinity, electron charge, dielectric constant of vacuum and electron–hole separation for the CT exciton, respectively. Using $E_I = 7.62$ eV (Beck *et al* 1996) and $E_A = 2.65$ eV (Wang *et al* 1991), and the observed exciton energies 2.92 eV (425 nm) for microcrystal beam and 2.76 eV (450 nm) for film, R is estimated to be 0.65 nm and 0.70 nm, respectively. This indicates that the photogenerated electron and hole face each other in adjacent C_{60} molecules. For a more detailed discussion of the CT exciton band with some structure, the contributions from the electron–vibration couplings, orientational disorder and configurational disorder in the C_{60} condensed system have to be taken into account. Using the Su–Schrieffer–Heeger Hubbard-type Hamiltonian, Salkola (1994) computed absorption spectra of a C_{60} molecule including both the direct and one-phonon-induced processes and explained the detailed structure of the CT exciton band. He obtained optical absorption spectra with several one-phonon peaks in the wavelength region between 400 nm and 540 nm and showed that the optical absorption intensities depend on the on-site Hubbard interaction parameter U/t (U: the on-site Coulomb interaction; t: the intra-molecular transfer energy of an electron). Although these absorptions are suppressed by strong electron–electron repulsion U in a C_{60} molecule, as observed for the C_{60} solutions (figure 8), with increasing size of C_{60} aggregate, the absorptions may be enhanced by the increase in the inter-molecular electron transfer, as shown in figures 1, 2, 3 and 4. On the other hand, attaching great importance to the pair

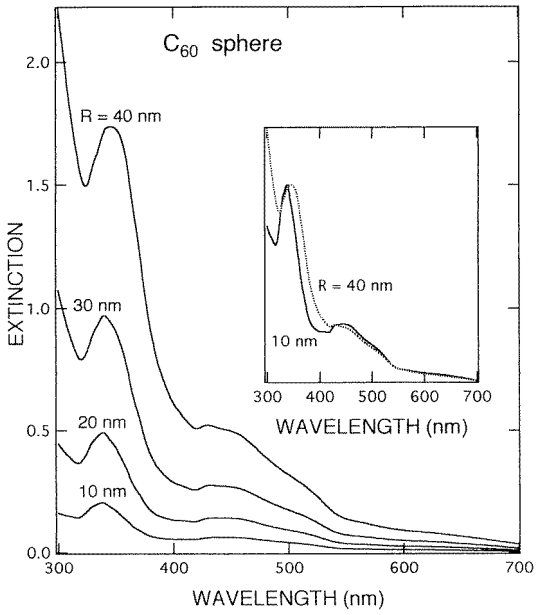

Figure 9. Calculated extinction cross section spectra of C_{60} spheres with different radii.

interaction between C_{60}^{+} and C_{60}^{-}, Jiang and Gan (1995) calculated the optical absorption spectra of C_{60} crystal with the Hubbard-type Hamiltonian. The result indicates that the CT exciton absorption grows and shifts toward the longer-wavelength side on increasing the parameter U/B (U: the on-site Coulomb interaction between a hole in C_{60}^{+} and an electron in C_{60}^{-}; B: the exciton band width). Therefore, the time evolution of the CT band shown in figures 1, 2, 3 and 4 may be explained by the increase in the exciton band width with increasing C_{60} crystallite size.

Also, we discuss the intensity peak shift in the h_g–t_{1u} transition during evaporation. It has been reported for C_{60} film formation on a substrate that the film consists of microcrystal islands at the early stage of evaporation and a uniform film is produced at the later stage (Tanaka *et al* 1993a, b). Therefore, in order to simulate the spectral evolution observed in the microcrystal, microcrystal beam and film experiments, we calculate the Mie extinction cross sections of a C_{60} sphere with various radii R using the reported dielectric constant of C_{60} single crystal (Milani *et al* 1994). The results are shown in figure 9. The extinction cross sections are expressed in units of the geometric cross section. With size increasing from 10 nm to 40 nm, the h_g–t_{1u} band shifts to the longer-wavelength region, and this is accompanied with spectral broadening, as observed in the present experiments. To show this more clearly, the spectra of spheres with radii of 10 nm and 40 nm are shown in the inset. They are normalized with respect to the intensity at the peak wavelengths of the h_g–t_{1u} band. We have also calculated the extinction cross section of C_{60} cubes of the same size, but no difference from the case of C_{60} spheres was observed. The shift and broadening arise from retardation effects.

The structure of the spectra and their time dependence obtained in our different types of experiment indicate the spectral evolution in C_{60} aggregate with increasing number of constituent molecules. Also, it is found that the CT absorption band shifts and becomes prominent with increasing size of the C_{60} system.

4.2. C_{60} microcrystal growth

We discuss the C_{60} microcrystal growth under confined- and flowing-gas conditions. Under confined-gas conditions, the following results are obtained.

(1) The optical extinction decreases with increasing pressure of the confined gas.

(2) It is more difficult to produce two vertically well separated vapour zones (transparent and smoky zones), and, even for high-pressure confined-gas conditions (150 Torr), the separation between the transparent zone and the smoky brown one is larger than 32 mm, which is much larger than the values for noble metals (Mochizuki and Ruppin 1993) and alkali metals (Mochizuki *et al* 1997).

Result (1) is always observed for the case of sublimation evaporation, which is trivial physically, since it is well known that the sublimation point rises with increasing confined pressure.

Result (2) may indicate that there is a large critical radius below which the crystallite is unstable under confined-gas conditions. The critical radius R_c at a given temperature is

$$R_c = 2V_m\sigma / k_B T \log S \tag{2}$$

where V_m, σ, k_B and S are the volume of the C_{60} molecule, the surface tension of condensed C_{60}, the Boltzmann constant and the supersaturation ratio, respectively (Abraham 1974). A glance at this equation convinces us that the large value of V_m for the C_{60} molecule gives a large critical radius, though the values of σ and S are not determined at present.

Under flowing-gas conditions, it was found that heavier gas is needed to produce a well-directed C_{60} microcrystal beam, as observed for other semiconductor evaporations (Mochizuki 1996, Mochizuki and Umezawa 1997). This is mainly due to the decreased mean free path of the C_{60} vapours in the heavier gas.

Acknowledgments

We should like to thank Professor Ryousei Uno and Professor Akira Ishikawa (The Institute of Natural Sciences of Nihon University) for their help in the x-ray diffraction and electron microscopic studies of C_{60} films and microcrystals. Also, we would like thank Mr Haruya Kitahara, Mr Shigeo Katoh and Mr Tohru Takahashi for their help in the early measurements. One of the authors (R Ruppin) is indebted to The Japan Society for The Promotion of Science for financial support (The Fellowship for Research in Japan).

References

Abraham F F 1974 *Homogeneous Nucleation Theory* (New York: Academic)

Beck R D, Weis P, Rockenberber and Kappes M M 1996 *Surf. Rev. Lett.* **3** 771

Capozzi V, Gasamassima G, Lorusso G F, Minafra A, Piccolo R, Trovato T and Valentini A 1996 *Solid State Commun.* **9** 853

Friedman B and Harigaya K 1993 *Phys. Rev.* B **47** 3975

Jiang X and Gan Z 1995 *Phys. Rev.* B **52** 14 254

Kataura H, Irie N, Kobayashi N, Achiba Y, Kikuchi K, Hanyu T and Yamaguchi S 1993 *Japan. Appl. Phys.* **32** L1667

Kazaoui S, Ross R and Minami N 1994 *Solid State Commun.* **90** 623

Lof R W, van Veenendaal M A, Koopmans B, Jonkman H T and Sawatzky G A 1992 *Phys. Rev. Lett.* **68** 3924

Milani P, Manfredini M, Guizzetti G, Malabelli F and Patrini M 1994 *Solid State Commun.* **90** 639

Mishori B, Katz E A, Faiman D and Shapira Y 1997 *Solid State Commun.* **102** 489

Mochizuki S 1996 *J. Lumin.* **70** 60

Mochizuki S and Ruppin R 1993 *J. Phys.: Condens. Matter* **5** 135
——1994 *J. Phys.: Condens. Matter* **6** 7303
Mochizuki S, Sasaki M and Ruppin R 1997 *J. Phys.: Condens. Matter* **9** 5801
Mochizuki S and Umezawa K 1997 *Phys. Lett.* **228A** 111
Nitta H, Suzuki M, Iida T and Nasu K 1997 *Mtg of the Physical Society of Japan* (Tokyo: The Physical Society of Japan) abstracts 52-1, part 1, p 298
Ohno K, Murayama M, Takahashi M, Yu J-Z, Gu B L and Kawazoe Y 1996 *Surf. Rev. Lett.* **3** 735
Ren S L, Wang Y, Rao A M, McRae E, Holden J M, Hager T, Wang K, Lee W, Ni H F, Selegue J and Eklund P C 1991 *Appl. Phys. Lett.* **59** 2678
Saito S and Oshiyama A 1991 *Phys. Rev. Lett.* **66** 2637
Salkola M I 1994 *Phys. Rev.* B **49** 4407
Su W P, Schrieffer J R and Heeger A J 1988 *Phys. Rev.* B **22** 2099
Tanaka N, Kitagawa T, Kachi T and Kizuka T 1993a *Ultramicroscopy* **52** 533
Tanaka N, Kitagawa T and Kizuka T 1993b *Mater. Sci. Eng.* B **19** 53
Tsubo T and Nasu K 1994 *Solid State Commun.* **91** 907
Yabana K and Bertsch G F 1992 *Chem. Phys. Lett.* **197** 32
Wang L S, Conceiao J, Jin C and Smalley R E 1991 *Chem. Phys. Lett.* **182** 5